Self-assembly of bis(phthalocyaninato)terbium on metal surfaces

2015 Phys. Scr. 90 098003

(http://iopscience.iop.org/1402-4896/90/9/098003)

IOP Publishing | Royal Swedish Academy of Sciences Physica Scripta

Phys. Scr. **90** (2015) 098003 (9pp) doi:10.1088/0031-8949/90/9/098003

Invited Comment

Self-assembly of bis(phthalocyaninato) terbium on metal surfaces

Zhitao Deng[1], Stephan Rauschenbach[1,5], Sebastian Stepanow[1], Svetlana Klyatskaya[2], Mario Ruben[2,3] and Klaus Kern[1,4]

[1] Max-Planck-Institute for Solid State Research, Heisenbergstr. 1, D-70569 Stuttgart, Germany
[2] Institute of Nanotechnology, Karlsruhe Institute of Technology (KIT), 76344 Eggenstein-Leopoldshafen, Germany
[3] IPCMS-CNRS UMR 7504, Université de Strasbourg, 23 Rue du Loess, 67034 Strasbourg, France
[4] Institut de la Matière Condensée Physique des Nanostructures, Ecole Polytechnique Fédérale de Lausanne, CH-1015 Lausanne, Switzerland

E-mail: s.rauschenbach@fkf.mpg.de

Received 12 March 2015, revised 15 June 2015
Accepted for publication 15 July 2015
Published 13 August 2015

Abstract

Single-molecule magnets represent the smallest stable magnetic entities available to technology, with promising applications in data storage and quantum computation in sight. Therefore, an interface between devices and single-molecule magnets must be developed, for which the self-assembly behavior at surfaces is highly relevant. The molecular magnet bis(phthalocyaninato) terbium ($TbPc_2$) represents a molecular system with interesting magnetic properties. In order to fabricate low dimensional nanostructures based on $TbPc_2$, the self-assembly behavior on Cu(100), Cu(111) and Au(111) substrates is studied in ultra-high vacuum (UHV). On Cu(100), $TbPc_2$ does not aggregate even at high coverage, which yields a good zero-dimensional system. On Cu(111), the $TbPc_2$ molecules self-assemble into ribbon-like islands with a high aspect ratio, or an isotropically growing phase, depending on the coverage. On Au(111), $TbPc_2$ molecules form two-dimensional domains from the initial growth stage and extend to highly ordered films, which cover entire terraces at high coverage. The molecular ordering of $TbPc_2$ can be understood based on the behavior of single Pc adlayers, taking into account the molecular double-decker structure. The freedom in the dihedral angle between top and bottom Pc ligands allows one to optimize the molecular ordering through a flexible conformation.

Keywords: bis(phthalocyaninato) terbium, scanning tunneling microscopy, molecular beam epitaxy, self-organized growth, single-molecule magnets, self-assembly

(Some figures may appear in colour only in the online journal)

Introduction

The ever-increasing density of modern data storage devices has reached dimensions where a single bit of information is stored in the direction of the magnetization of a metal nanostructure with a lateral size of a few tens of nanometers. This is made possible by the engineering of magnetic materials with high magnetic anisotropy energies. Current technology approaches the limit in magnetic anisotropy while, at the same time, quantum size effects start to play a role in the nanometer sized objects. In the search for new materials, synthetic approaches based on coordination chemistry have provided a new class of materials, i.e. single-molecule magnets (SMMs) [1, 2].

Single-molecule magnets are well-defined entities consisting of one or more metal ions that are held together by

[5] http://fkf.mpg.de/kern/

organic ligands. Hence they possess a well-defined stoichiometry and atomic structure. The metal ions carry spins, which couple through the organic ligands, yielding a so-called giant spin with particular energy levels and a high magnetic anisotropy barrier. Their most prominent feature is the slow relaxation of magnetization at low temperatures that sets in, for relaxation times comparable to technologically relevant time scales, below the so-called blocking temperature. Due to their inherent nanoscale dimensions quantum effects play a major role in these compounds [3]. The magnetization can coherently rotate and relax due to spin quantum tunneling, rendering these systems also promising for quantum computation and related quantum information processing devices.

A variety of transition metal as well as lanthanide and actinide based SMMs with ring shapes or as compact clusters have been synthesized, however the blocking temperatures have not exceeded a few degrees Kelvin. With the development of phthalocyanine-based magnets comprising a single lanthanide ion the blocking temperature was boosted to a couple of tens of Kelvin [4–7]. These single-ion magnets feature a lanthanide ion sandwiched between two parallel phthalocyanine macrocycles. The highly symmetric coordination environment results in strong crystal field splitting of the lowest high-J multiplets with thermal magnetization reversal barriers up to 100 K. The lanthanide complexes also show inherent quantum tunneling of magnetization limiting their magnetic bistability [8, 9]. The so-called double-decker complexes have been synthetically modified with specific effects on the relaxation rate and quantum tunneling [10, 11]. In particular, the redox state of the macrocycle ligand appears to be important for the magnetic relaxation near zero field.

Single-molecule magnets are an interesting class of compounds for the development of molecular spintronics devices [12]. Their incorporation into functional architectures requires the contact of SMMs to solid surfaces [13–15]. Much effort was dedicated to depositing SMMs onto various substrates, however, the fragile nature of most SMMs leads to decomposition of the molecules in the process of deposition or the deterioration of the magnetic properties [16, 17], only avoidable by extensive technological efforts such as electrospray ion beam deposition [18]. This problem has been largely overcome with the use of the very stable lanthanide double-decker molecules, which mostly preserve their properties when in contact with a solid [19–23]. This has also spawned a series of investigations of the local spin and electronic properties of individual double-decker molecules adsorbed on well-defined crystalline surfaces [24–32].

Apart from the investigation of the properties of individual double-decker complexes, these three-dimensional molecules are also interesting as molecular building blocks in self-assembled monolayers. Already in simple metallo-phthalocyanine (Pc) the functional site, which is the coordinatively bound metal ion, is separated from the surrounding molecular scaffold. This building principle leads to a versatility which allows for a wide variety of applications, ranging from the major use of Pc as dye in pigments [33] to applications in organic field effect transistors, gas-sensing devices [34, 35], as photovoltaic materials, and light-emitting diodes [36, 37].

In double-decker complexes, i.e. metal-di-Phthalocyanines (MPc_2), a lanthanide atom is placed in between two Pc ligands, with a 4-fold coordination of the metal atom to each of the Pcs [38, 39]. A central lanthanide atom can be freely chosen during the synthesis in order to change the spin and electronic configuration of this molecular entity. Due to its particular shape these molecules are dubbed *double-decker*. The high spin double-decker Pcs, such as $TbPc_2$, are single molecule magnets exhibiting a high blocking temperature [6, 40, 41]. $TbPc_2$ molecules possess large magnetic anisotropy and show slow relaxation of their magnetic moment. As their magnetic properties are largely preserved when adsorbed on the surface [19], they are good candidates for potential applications as SMMs in nano electro-magnetic devices, which has recently been demonstrated in several instances.

For such application the immobilization and agglomeration at a solid surface is crucial. Structure and conformation of the adsorbed molecules as well as interactions, both mutual between molecules and with the surface, often have a great influence on the molecular properties. Particularly, the double-decker system adsorbed to a solid surface represents a promising route towards the fabrication of low dimensional, molecular, magnetic systems, due to the independent tunability of the components.

Here we present an adsorption and self-assembly study of the neutral form of bis(phthalocyaninato) terbium ($TbPc_2$) on different metal surfaces. Scanning tunneling microscopy (STM) in ultrahigh vacuum enables us to characterize the adsorbed molecules with submolecular resolution. We use atomically defined crystalline surfaces of gold and copper: Cu(100), Cu(111), and Au(111). These surfaces differ in surface potential corrugation and symmetry, which leads to a series ranging from reactive, strongly interacting Cu(100) to rather inert Au(111). Different molecular coverages for the STM investigation were prepared using a calibrated vacuum evaporation source. The substrate temperature was varied between room temperature and 40 K to control the thermal diffusion of the molecules at the surface. Under these conditions we are able to image individual molecules, molecular agglomerations in two dimensions, multilayered structures, defects and grain boundaries, as well as the surface's atomic structure for reference.

The molecular ordering of (metallo-)phthalocyanines (MPcs) has been studied intensively. This class of molecules already presents a rich variety of self-assembly phenomena. They can form highly ordered, commensurate adlayers on Au(111) [42, 43], as well as a variety of non-commensurate adlayer structures on the Cu(111) surface, which is expressed in the anisotropic charge transfer between Cu(111) and Pcs [44–47].

The double-decker geometry adds an interesting complication to the molecular ordering in adlayer films. The interaction with the surface leads to a symmetry breaking in the molecule, which has been detected for individual molecules on surfaces [25, 26]. The intermolecular interaction

between double-decker molecules is expected to be stronger as compared to single Pc adlayers due to the two parallel stacked Pc ligands. Moreover, in Pc double-deckers the central ion is acting as a semi-flexible joint, allowing for nearly free twisting between top and bottom Pc. In bulk crystals this angle is found ranging from 6° to an ideal 45° depending on the central atom [47]. This additional degree of freedom can have a significant influence on the self-assembly of $TbPc_2$ on surfaces and may further be responsible for the observation of different magnetic relaxation times due to symmetry breaking with dihedral angles different from 45°.

Materials and methods

$TbPc_2$ synthesis

A neutral form of $TbPc_2$ was obtained by making several modifications to the protocol based on the published procedure reported in [48, 49]. The synthesis was accomplished by templating reactions, starting from a mixture of the phthalonitrile precursor o-dicyanobenzene and the terbium acetylacetinate $Tb(acac)_3{\cdot}nH_2O$, in the presence of a strong base (e.g. DBU, alkoxides) and high-boiling solvents, such as pentanol or hexanol. A mixture of 1,2-dicyanobenzene (42 mmol), $Tb(acac)_3{\cdot}4\,H_2O$ (5 mmol), and 1,8- diazabicyclo [5,4,0] undec-7-ene (DBU) (21 mmol) in 50 ml of 1-pentanol was refluxed for 36 hours. The solution was allowed to cool down to room temperature before adding acetic acid and reheating at 100 °C for 0.5 h. The precipitate was collected by filtration and washed with n-hexane and Et_2O. The crude purple product was again dissolved in 800 ml of $CHCl_3$/MeOH (1/1) and undissolved PcH_2 was filtered off. Both forms, blue (anionic $[TbPc_2]^-$) and green (neutral $[TbPc_2]^0$), were obtained simultaneously, as revealed by electronic absorption spectra [38, 39] In order to convert the unstable anionic form into the neutral one, the reaction mixture was presorbed on active (H_2O-0%) basic alumina oxide. Purification was obtained by column chromatography on basic alumina oxide (deactivated with 4.6% H_2O, level IV) with chloroform/methanol mixture (10:1) as an eluant. Analytically pure powder samples were obtained with 30% yield. Deep green crystals of the products can be produced by using slow diffusion of CH_2Cl_2 into $C_2H_2Cl_4$ solution of the pristine material. The $TbPc_2$ crystallized in the space group $P2_12_12_1$ (γ-phase) the same way as reported by Takeya *et al* [50].

Scanning tunneling microscopy

Sample preparation and scanning tunneling microscopy (STM) investigations were carried out in a combined ultra-high vacuum (UHV) molecular beam epitaxy (MBE) and variable-temperature STM system (Omicron Nanotechnology, Taunusstein, Germany). The base pressure in the system was lower than 2×10^{-10} mbar. Prior to each adsorption experiment, the Cu(100), Cu(111) and Au(111) single crystals were cleaned by repeated cycles of Ar^+ sputtering (15 μA, 1 keV, 15 min) and subsequent annealing at 800–900 K for 15 min.

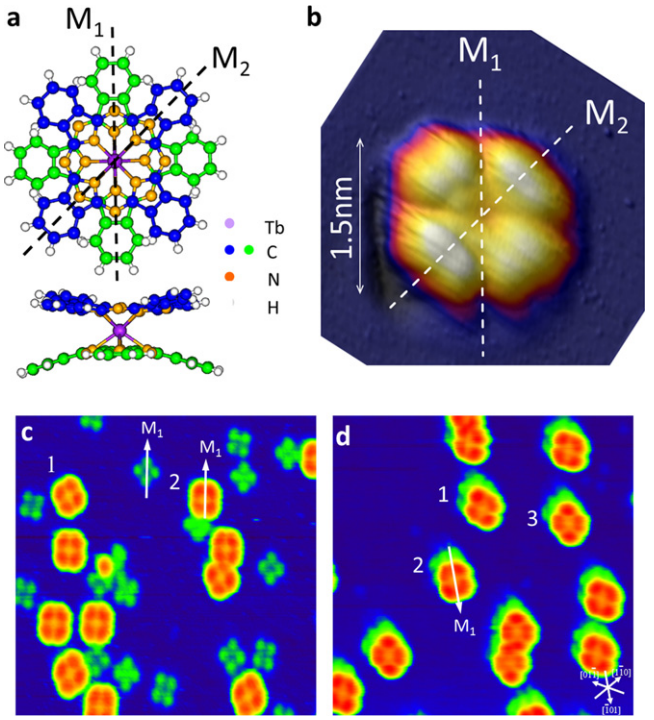

Figure 1. Individual $TbPc_2$. (a) Chemical structure of the $TbPc_2$ molecule. M_1 and M_2 are the symmetry axes of the bottom Pc ligand (green). (b) STM topograph of a single $TbPc_2$ molecule on Cu(100) measured at 300 K. $TbPc_2$ is imaged as four bright lobes. ($U_{bias} = -1.0$ V, $I_t = 100$ pA, 4 nm × 4 nm). (c) $TbPc_2$ (four bright lobes) and free Pcs (four lobes with lower contrast) on Cu(100) measured at 300 K. Two molecule orientations can be observed. ($U_{bias} = -2.0$ V, $I_t = 100$ pA, 15 nm × 15 nm). (d) STM topograph of isolated $TbPc_2$ molecules on Cu(111) measured at 45 K. In total three orientations of molecules can be observed. ($U_{bias} = -1.5\,V$, $I_t = 80$ pA, 15 nm × 15 nm).

To confirm their cleanliness, the bare gold and copper surfaces were imaged before the deposition of the molecules. The $TbPc_2$ molecules were evaporated from a crucible heated to 760 K onto a substrate held at room temperature with a deposition rate of approximately 0.02 ML per minute. Despite the complex molecular structure of $TbPc_2$ we find that it can be thermally evaporated onto metal surfaces without decomposition [19]. By controlling the deposition time, molecular layers of different coverage were prepared. After deposition the Cu(111) and Au(111) substrates were cooled to 40 K and STM constant current topography images were recorded. At low temperature (40 K) the mobility of $TbPc_2$ molecules on Cu(111) and Au(111) surfaces is greatly reduced, allowing the study of nucleation and growth of the molecular layers in detail. The adsorption of $TbPc_2$ on Cu(100) was studied at room temperature. The bias voltage is applied to the STM tip.

Results

Isolated $TbPc_2$ on Cu(100)

The molecular structure of a free $TbPc_2$ is sketched in figure 1a with the carbon atoms in the different Pc ligands marked

by blue and green color. In an adsorbed molecule they correspond to the top and bottom Pc ligand, respectively. M_1 and M_2 denote the symmetry axes of the bottom Pc ligand (green), with M_1 given by the symmetry axis along the benzene groups. The lateral dimension of $TbPc_2$ is about 1.5 nm measured along the indicated M_1 axis and its height is about 0.4 nm. The free molecule is characterized by a fourfold (D_{4d}) symmetry inherited from the Pc ligands. In bulk crystals of $TbPc_2$, however, the 4-fold symmetry is broken and the Pc ligands are rotated by 41.4° with respect to each other [50].

Panels (b)–(d) of figure 1 show the STM topography of isolated $TbPc_2$ molecules on Cu(100) and Cu(111) surfaces. The molecules adsorb with one Pc ligand on the surface and are imaged as four bright lobes corresponding to the top Pc ligand [24, 50]. The lateral dimensions of 1.4 nm by 1.4 nm and the apparent height of 0.4 nm are in agreement with the size of the $TbPc_2$ molecule. Additionally, individual Pcs with an apparent height of 0.15 nm are found on the surface (figure 1(c)). This surplus of free Pcs can be eliminated by thorough degassing of the evaporator at 760 K after which only $TbPc_2$ molecules were found on the surface (figure 1(d)).

On the Cu(100) surface, $TbPc_2$ molecules do not form ordered agglomerations, neither at higher coverage of up to 0.6 ML nor after post-deposition annealing up to 600 K. A strong interaction between the Cu(100) surface and the $TbPc_2$ molecules immobilizes the molecules completely. This is supported by a clear STM imaging at room temperature of $TbPc_2$, which is possible on Cu(100) but not on Cu(111). Similar observations have been reported for FePc, CuPc, and CoPc on Cu(100) [46].

Two adsorption configurations, identical but rotated by 45°, can be identified for the $TbPc_2$ as well as for the free Pc on Cu(100) (figure 1(c)). The four-lobes of the $TbPc_2$ STM-topography, which represent the electronic structure of the top Pc ligand [24, 50], are undisturbed symmetrically. We conclude that the dihedral angle between the two ligands is approximately 45° for the isolated $TbPc_2$. The cross depression in the STM topography of $TbPc_2$ can be interpreted as the M_1 axis of the lower ligand (marked by white arrows in figure 1(c)), while the orientation of the four lobes defines the M_2 axis.

Miyake *et al* reported that the top Pc ligands can jump among four equilibrium orientations [51]. Thereby the equilibrium dihedral angle of ideally 45° is influenced by the environment. Even though metallo di-Phthalocyanines (MPc_2) show a wide range of dihedral angles in bulk crystals [47], for isolated $TbPc_2$ molecules the lateral external influence is negligible and the equilibrium dihedral angle is 45°, which agrees with our observations.

Submonolayer and monolayer of $TbPc_2$ on Cu(111)

At low coverage (< 5% of a monolayer) $TbPc_2$ molecules are found individually dispersed on Cu(111) after cooling the substrate to 40 K. We find three preferential orientations (figure 1(d)) and an undisturbed symmetry of the molecules, which points to a dihedral angle between the two Pc ligands close to 45°. This allows us to identify the orientation of the molecule with respect to the principal directions of the Cu(111) surface. The M_1 axis is aligned to one of the surface principal directions. This adsorption geometry is known as the most stable configuration of MPc on Cu(111) [45, 46]. Because the surface corrugation potential of the close-packed Cu(111) surface is lower than the less densely packed Cu (100) surface, $TbPc_2$ is mobile on Cu(111) at room temperature [52]. Consequently at higher coverage the $TbPc_2$ aggregates into ordered structures (figure 2).

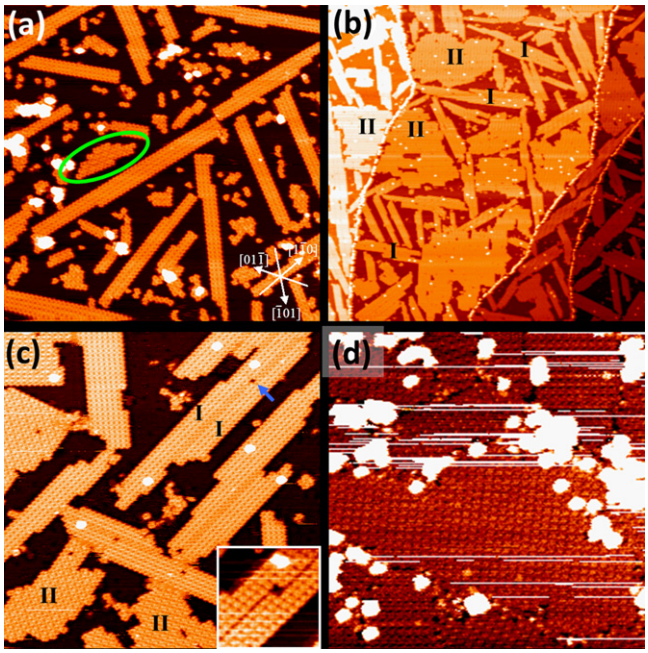

Figure 2. $TbPc_2$ on Cu(111) at increasing coverage. (a) Topography image of 0.5 ML of $TbPc_2$ shows that molecules tend to aggregate along six directions on Cu(111). The green ellipse marks an island different from ribbon-like islands. ($U_{bias} = -2.0$ V, $I_t = 80$ pA, 100 nm × 100 nm). (b) Constant current topography of $TbPc_2$ submonolayer on Cu(111) with a molecular coverage of 0.8 ML, showing large two-dimensional and ribbon like islands. ($U_{bias} = -2.0$ V, $I_t = 100$ pA, 320 nm × 320 nm). (c) STM topography of a $TbPc_2$ submonolayer (0.8 ML) on Cu(111). Two phases exhibiting different patters are visible. ($U_{bias} = -1.5$ V, $I_t = 100$ pA, 80 nm × 80 nm) The inset image shows the magnified gap (at the blue arrow) between two adjacent phase I islands ($U_{bias} = -1.5$ V, $I_t = 100$ pA, 14 nm × 14 nm). (d) Full monolayer $TbPc_2$ on Cu(111) ($U_{bias} = 2.0$ V, $I_t = 100$ pA, 50 nm × 50 nm).

At about 0.5 ML, the molecules form elongated, ribbon-like islands that exhibit a characteristic superstructure (figure 2(a)). The long axis of these islands is oriented along six directions making an angle of ±10° with respect to the high symmetry directions of the Cu(111) surface. The width of the ribbons is limited to four rows, whereas their length can be much larger and easily exceed 50 nm. This implies an anisotropic growth during $TbPc_2$ island formation. At a coverage below 0.5 ML we observe almost exclusively ribbon-islands. Besides the ribbons we find a second type of small, structurally different islands at low abundance, one example of which is highlighted by a green ellipse in figure 2(a). In the following, the two different types of islands are denoted as phase I for the ribbons and phase II for this second type.

With increasing coverage the relative share and size of the phase II islands increases. At a coverage of 0.8 ML (figure 2(b), (c)) more than 60% of the molecule-covered surface area belongs to phase II domains. These islands grow isotropically and have diameters comparable to the length of the phase I ribbons. Moreover, phase I and phase II islands differ in their orientation with respect to the substrate lattice. In the STM topography they can further be distinguished by a different grid-like superstructure, which points towards structural differences between those two phases.

Figure 2(c) shows a detailed view of both types of islands at 0.8 ML coverage. Broad phase I islands show a linear depression dividing them into two ribbons of a width of up to four rows, indicating that they are composed of two adjacent yet unmerged phase I ribbons (inset figure 2(c)). Wide phase I ribbons without a depression line are found as well, but are very rare.

At 1 ML coverage we find a closed molecular film (figure 2(d)) consisting of domains of exclusively phase II islands, separated by clearly visible, rugged domain boundaries, exposing sizable voids. Several excess molecules on top of the first monolayer cluster at these grain boundaries. All of the domains show the characteristic superstructure of phase II at different orientations, as well as the isotropic shape with island sizes around 50 nm. No features of phase I islands can be found.

$TbPc_2$ on Au(111)

On the Au(111) surface, transition metal Pcs—closely related to $TbPc_2$—such as FePc, NiPc, CuPc, and CoPc, self-assemble into highly ordered, commensurate adlayers [42, 48, 49]. $TbPc_2$ is mobile on Au(111) at room temperature. It nucleates into small islands of rectangular shape when a low molecular coverage of approx. 0.1 ML is cooled to 40 K (figure 3(a)). These islands are aligned with the corrugation of the Au(111) surface reconstruction: their long edge encloses an angle of 15° with the $[11\bar{2}]$ direction.

At a higher coverage we observe larger islands as well as fully covered terraces, shown in figure 3(b) for 0.5 ML and figure 3(c) for 0.9 ML. Large agglomerations are the result of merging islands that have nucleated on the same terrace of the Au(111) surface. The island displayed in figure 3(b) for instance contains several small voids, reminiscent of the coalescence of several islands. At higher coverage these holes are filled with mobile molecules from higher molecular layers, eventually becoming trapped in the voids. Some excess molecules remain in the second layer at high coverage (0.9 ML), shown in figure 3(c). Note that the orientation of these molecules depends on the orientation of the domain underneath.

Even though the large islands in figures 3(b) and (c) may appear to be single crystalline, they are in fact composed of several domains. Two types of very smooth, compact, domain boundaries, **A** and **B**, are indicated in figure 3(c). At the type **A** boundaries the superstructure appears to be shifted by half a period, which we highlighted by lines crossing the boundaries. Type **B** boundaries separate domains that are mirror symmetric. This is only seen either by inspecting the edges, where single molecules are apparent and reveal their orientation (yellow arrows), or from the orientation of the second layer $TbPc_2$.

Molecular arrangement of islands and superstructures

The internal structure of the three types of $TbPc_2$ domains, one on Au(111) and phase I and II on Cu(111) is obscured by the convolution of molecular features of neighboring top Pcs. In addition, we observe superstructures, which are characteristic for each type of domain, caused by the molecular arrangement and the interaction with the surface. Nevertheless, characteristic features of the $TbPc_2$ molecules are observable in the islands and can be used to decipher the molecular ordering.

The phase I islands on Cu(111) show a square lattice periodicity with lattice vectors $|\mathbf{A}_1| = |\mathbf{A}_2| = (14 \pm 1)$Å (figure 4(a)). In the magnified image of phase I, additionally a zigzag shaped reconstruction is observed. Even though the individual $TbPc_2$ molecules cannot be directly identified, the unit cell is consistent with their shape and size. According to the observation of the isolated $TbPc_2$, the centers of the molecules are imaged as dark spots, which we apply for the interpretation of the island topography. The unit vector $\mathbf{A}_1$ is parallel to the long edge of the island and thus makes an angle of 10° with the $[1\bar{1}0]$ direction of Cu(111).

The orientation of the $TbPc_2$ molecules is deduced by a careful inspection of the island edges. Yellow arrows point out some of the periodically occurring notch-like features that represent part of a cross-like depression of each molecule (figure 4(a)). All notches point into the same direction, aligning one M_1 axis of $TbPc_2$ parallel to the $[\bar{1}01]$ direction of Cu(111) as sketched in figure 4(d). This alignment is consistent with the configuration of Pcs on Cu(111) surfaces reported in the literature [46, 48].

We further applied the same approach to determine the molecular arrangement in the phase II molecular layers on Cu(111) and also to the $TbPc_2$ films on Au(111). The structural details of a phase II island are shown in figure 4(b). Again we identify the array of dark protrusions with the center of the molecule, which is consistent with the molecules' dimensions of 1.4 nm × 1.4 nm. In contrast to phase I, the superstructure (indicated by the dotted box in figure 4(b)) is larger than a single molecule: neighboring dark spots in phase II do not repeat exactly the same features.

The analysis of the island's edges is consistent with this observation. Alternating notch features of different orientation (pointed out by yellow and blue arrows in figure 4(b)) can be identified at the island's boundary. This pattern suggests a compound lattice for phase II with two molecules per unit cell. We compare the orientation of the notches with the principal directions of Cu(111) and find that the M_1 axis of configuration (1) (light blue) and (2) (dark blue) both align with close-packed, principle direction of the substrate, which are $[01\bar{1}]$ and $[\bar{1}01]$, respectively (figure 4(e)). The molecules are arranged in a square lattice with parameters $|\mathbf{B}_1| = |\mathbf{B}_2| = (20 \pm 1)$Å.

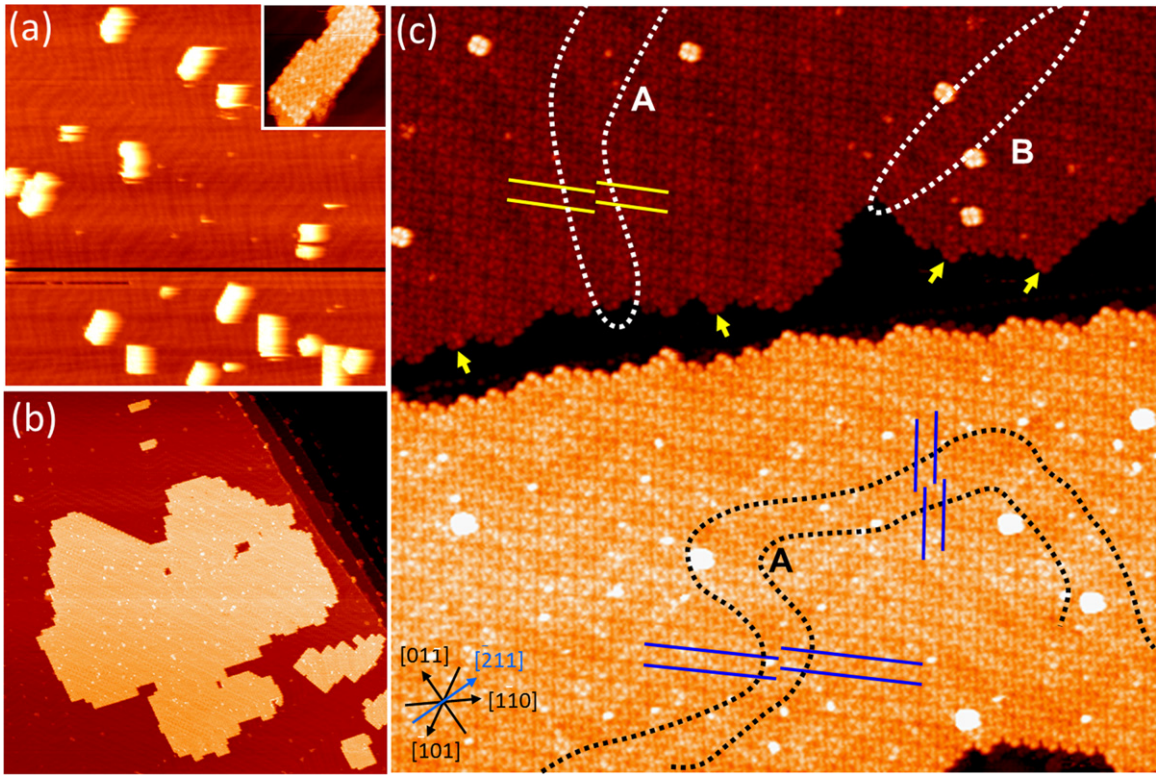

Figure 3. Different Coverage of $TbPc_2$ on Au(111) (a) STM topograph of the initial growth stage (0.1 ML) of $TbPc_2$ on Au(111). Rectangular islands aligned with the reconstruction form on the terrace. ($U_{bias} = -2.0$V, $I_t = 60$ pA, 200 nm × 200 nm). Inset: magnified island. ($U_{bias} = -1.0$ V, $I_t = 60$ pA, 20 nm × 20 nm). (b) Two-dimensional islands of $TbPc_2$ at a coverage of 0.5 ML. ($U_{bias} = -2.0$V, $I_t = 100$ pA, 200 nm × 200 nm). (c) Topography of an almost full monolayer (0.9 ML) of $TbPc_2$ on Au(111). Large islands cover the entire terrace. The highlighted areas indicate domain boundaries. Yellow arrows indicate where the orientation of the molecules is visible at the island's edge ($U_{bias} = -2.0$ V, $I_t = 60$ pA, 100 nm × 100 nm).

At first glance, the structure of the $TbPc_2$ islands on Au (111) appears to be equivalent to phase II on Cu(111). In the magnified STM topography shown in figure 4(c) a similar superstructure of the same periodicity is observed. However, at the close-packed edge of the island's boundary, adjacent molecules are identically orientated (see also figure 3(c)). The M_1 axis of the molecule is aligned with $[01\bar{1}]$ direction of the Au(111) surface. Our observation of uniform orientation at the island's edge agrees with other tentative models for $TbPc_2$ [25] and the very similar YPc_2 [50] on Au(111). Our analysis yields a square lattice arrangement with the lattice parameters being $|\mathbf{C}_1| = |\mathbf{C}_2| = (14 \pm 1)$Å. The basis vector $\mathbf{C}_1$ is rotated by 15° with respect to the direction $[1\bar{1}0]$ of the Au(111) surface. A schematic model of the $TbPc_2$ molecular structure on Au(111), assuming the alignment of the M_1 axis with one of the Au(111) principle directions, is shown in figure 4(f).

In this tentative structure for $TbPc_2$ on Au(111), all molecules have the same orientation. The domains, in contrast, exhibit a pattern with a periodicity that corresponds to a unit cell containing two molecules in a square lattice, similar to the structure of phase II on Cu(111). One superstructure feature is indicated by the dashed square in figure 4c. Unlike two completely different molecular orientations in the unit cell of phase II, only a subtle symmetry break can be the cause of the superstructure on Au(111), since we know from the island edge that all molecules have the same orientation. The most likely explanation is thus a rearrangement of the angle between top and bottom Pc ligand. The adsorption position of one molecule in the lattice is defined by the interaction of the alignment of the lower Pc with one of the close packed lattice directions of the Au(111) surface and the mutual interaction with the neighboring lower-Pcs. To optimize the intermolecular interaction the molecule can twist the upper Pc, while the lower is fixed in its optimal adsorption conformation. In a simple scenario the top Pc ligand of one $TbPc_2$ molecule rotates clockwise while for the nearest neighbors the rotation is anticlockwise. While this is only a subtle change, which could not be detected by studying the island's edges, it constitutes a unit cell containing two molecules. In comparison, phase II of $TbPc_2$ on Cu(111) uses the same principle for optimizing the intermolecular interaction, but is rotating the entire molecule.

The behavior of the domain boundaries supports the picture of a subtle symmetry break, either by twisting the upper versus lower Pc or rotation of the entire molecule, as reason for the apparent superstructure. Two types of domain boundaries on Au(111), **A** and **B**, are visible in figure 3(c). In the upper part, the $TbPc_2$ molecules in the left and middle domains have the same orientation, which can be deduced from the edge of the island. The same is true for the whole terrace in the lower half. Nevertheless domain boundaries—marked by dotted lines labeled **A**—are visible within these domains. Along both

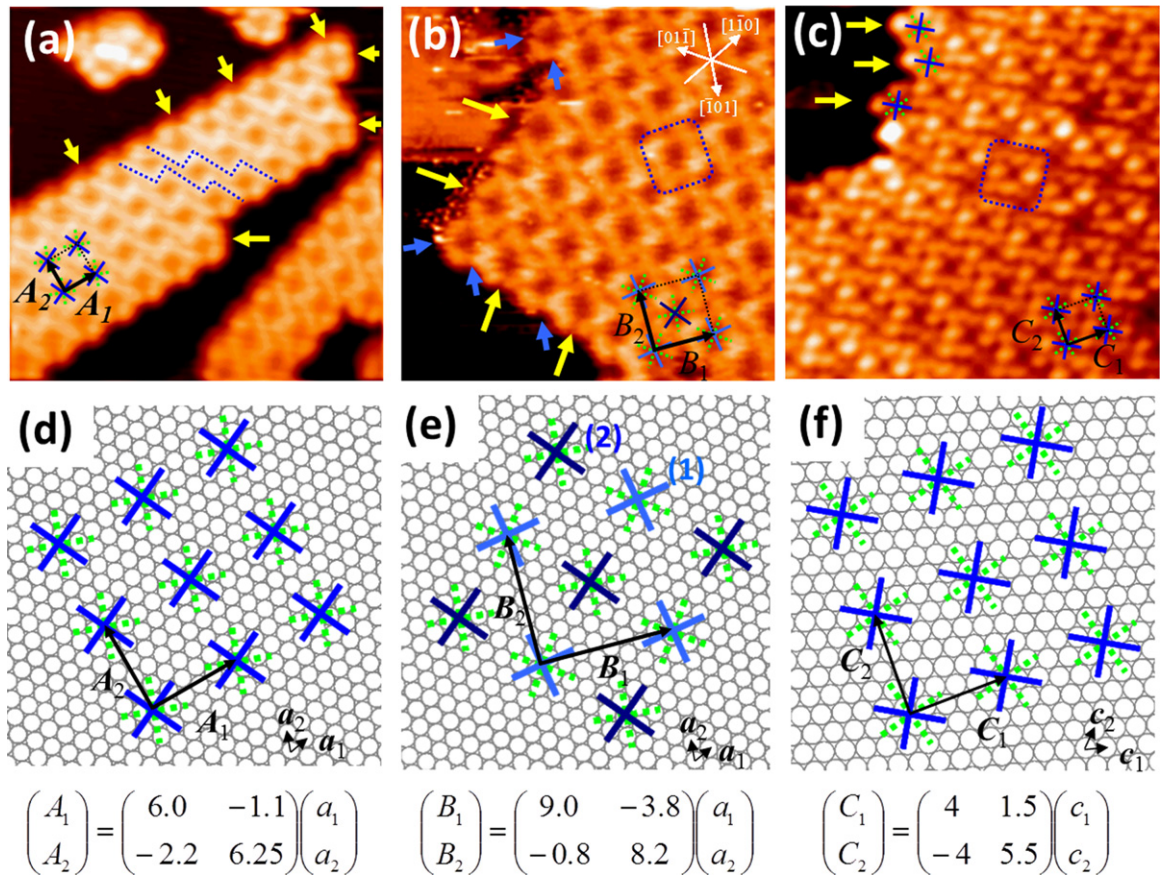

Figure 4. High resolution STM images and molecular structure models for $TbPc_2$ Cu(111) and Au(111). (a) Phase I on Cu(111). Yellow arrows point out the periodic features along the island edge. The dotted line indicates the zig-zag superstructure ($U_{bias} = -2.5$ V, $I_t = 180$ pA, 15 nm × 15 nm). (b) Phase II on Cu(111). Yellow and blue arrows point out some of the notch features at the island edge. The dotted square indicates the repeating unit of the superstructure. ($U_{bias} = -1.5$ V, $I_t = 100$ pA, 12 nm × 12 nm). (c) $TbPc_2$ monolayer on Au (111). The yellow arrows point out three molecules that help elucidate the orientation of $TbPc_2$ molecules. The dotted square indicates the apparent superstructure. ($U_{bias} = -1.5$ V, I_t=150 pA, 12 nm × 12 nm). (d)–(f) Schematic models for (a)–(c). The green and blue crosses represent the bottom and top Pc ligands. Vectors $\mathbf{a}_1$ and $\mathbf{a}_2$ are the primitive lattice vectors of Cu(111) surface, ($|\mathbf{a}_1| = |\mathbf{a}_2| = 2.55$Å) with an angle of 60° between them. Vectors $\mathbf{c}_1$ and $\mathbf{c}_2$ are the primitive lattice vectors of the Au(111) surface, ($|\mathbf{c}_1| = |\mathbf{c}_2| = 2.86$ Å) with an angle of 60° between them.

directions of the grid, the separated domains differ by a shift of precisely half of the superstructure dimension, highlighted by yellow and blue lines. This shift of (for instance) $\frac{1}{2}(\mathbf{C}_1 + \mathbf{C}_2)$ corresponds to exactly one molecular row of the $TbPc_2$ lattice, which means that both domains are identical with respect to molecular arrangement but only differ in the symmetry breaking that defines the appearance of the superstructure. Hence, the domain boundaries of type **A** can be interpreted as a mismatch of the periodic torsion of (at least) the top Pc ligands, which shifts the superstructure by one molecular row, i.e. the observed shift of half the pattern periodicity. In contrast, the domains at the type **B** boundaries are mirrored with respect to each other. This is best spotted by inspecting molecules at the island's edge as well as by the orientation of the isolated second layer $TbPc_2$.

In contrast to the pronounced superstructure of $TbPc_2$ on Au(111), the STM images of both phases of $TbPc_2$ on Cu(111) can be explained by a model assuming an angle of 45° between the two Pc ligands. Nevertheless, also here additional superstructures are observed, which are not predicted by the molecular structure of unperturbed $TbPc_2$ molecules and might be due to the rotational freedom of the torsion angle of $TbPc_2$. In phase I ribbons and in phase II islands a modulation in the brightness of the lobes can be observed, which should not be present in an ideal square lattice. The superstructure in phase I is indicated by dotted lines in figure 4(a). In figure 4(b) a dotted square shows one unit cell of the phase II structure, showing lobes of different brightness.

A precise torsion angle of the double-decker cannot be determined by the presented STM measurements of $TbPc_2$ molecules in densely-packed molecular layers due to the very close proximity of the topographic features of neighboring molecules. However, the twisting of the molecule would rather introduce a slight asymmetry in each lobe of the $TbPc_2$ STM topography, as for instance observed by Komeda *et al* [25]. Within a molecular lattice, this would be reflected in the STM images as a superstructure like the grid pattern on Au(111).

Discussion and conclusions

The free terbium double-decker is a highly symmetric molecule, as illustrated in figure 1(a). In our STM investigations we found a rich variety of (self-assembled) structures of the $TbPc_2$, ranging from individual molecules to large, very well ordered domains presenting complex superstructures. Resolving these structures at the submolecular level provides insight in the interrelation of the molecular degrees of freedom and intermolecular interactions.

An important feature of the molecule is that the top Pc ligand is electronically decoupled from the metal surface, which can be shown by density functional theory calculations [24] and is further expressed in the submolecularly resolved electronic structure exhibited by isolated $TbPc_2$ molecules on Cu(100) and Cu(111) [24]. Due to the straightforward preparation of individual $TbPc_2$ on Cu(100) at room temperature, this zero-dimensional system is interesting for probing of the magnetic properties of double-deckers as single molecules magnets. For instance, the magnetic anisotropy of the Tb ions of surface-supported single $TbPc_2$ molecules was investigated by x-ray magnetic circular dichroism (XMCD) [19].

The chemical structure of $TbPc_2$ suggests only weak intermolecular interaction. $TbPc_2$ has no pronounced binding sites for strong, directed, non-covalent interactions such as hydrogen bonds, ionic binding or complex coordination [53, 54]. Possible weak hydrogen bonds between the nitrogen atoms and the phenyl rings are highly unlikely due to a very long bond distance of approximately 0.3 nm [55–57]. Furthermore, a charge transfer between the lower Pc ligands and the metal surface must be taken into account. This is known to cause a symmetry breaking in the molecule , which leads to an additional dipole–dipole intermolecular interaction. Besides that, the interaction between neighboring Pc ligands has to be attributed to mainly dispersive van der Waals forces. However, the central atom allows for the top and bottom Pc ligands to be twisted away from the ideal 45° angle with respect to each other. For this a symmetry breaking is required, for instance due to the binding with neighboring molecules, as observed in bulk crystals.

$TbPc_2$ is aligned with principal substrate directions on both Cu substrates as well as on Au(111). This speaks for a strong interaction with the surface. It can thus be assumed that the binding distance for neighboring $TbPc_2$ is never exactly fitting for the unperturbed molecule. Consequently, the torsion angle will be adjusted to optimize the intermolecular bonding. While the direct observation of this twist is not possible, this symmetry breaking between top and bottom Pc ligand is the most plausible explanation for the superstructures observed on Au(111) and phase I on Cu(111) and also for the unique line defects observed on Au(111).

For phase II on Cu(111) another mechanism for symmetry reduction is likely to play an important role. The surface induces a symmetry reduction of Pcs, which has been reported in several works [44, 46]. The two pairs of the Pc's arms, which are parallel or vertical to the substrates principal direction are partially charged with opposite polarity [45]. It is favorable for these partial charges to interact strongly, which is the cause of the two-molecule unit cell of the phase II islands, observable in the pronounced superstructure.

Another consequence of this symmetry reduction by anisotropic charging of the bottom Pc ligand could be the pronounced anisotropic growth of phase I. For similar systems, such as CoPc on Cu(111), anisotropic growth of single row molecular chains has been observed. The limitation to four molecular rows of $TbPc_2$ additionally suggests an incommensurability with the substrate as contributing factor.

At low and medium coverage of $TbPc_2$ on Cu(111) almost exclusively phase I ribbons are observed. At high coverage the Cu(111) surface is increasingly covered by phase II islands until we find only phase II for the whole monolayer. By comparing the unit cell size, the density of both phases is approximately the same. Phase I ribbons, however, are separated by extended gaps, which is not favorable at higher coverage. Moreover, phase II does not show anisotropic growth, which allows its domains to grow further than phase I ribbons, which have already self-passivated their fast growing facet by reaching a neighboring domain. Hence, energetics and kinetics favor phase II at high coverage.

In summary, the judicious choice of the substrate proved to be an efficient way to control the mutual arrangement of Pc double-deckers. Even though the molecule itself has a very high symmetry, the interplay of molecule–substrate and intermolecular interaction leads to complex superstructures. In particular, the torsion angle freedom proves to be central for adopting the molecules to the substrate by subtle symmetry breaks, allowing us to produce large scale, high quality layers.

In principle, conformational freedom can be expected in large, complex molecules, however, it received little attention in studies of growth and self-assembly until now. Recent advances in surface preparation, namely the implementation of soft-landing electrospray ion beam deposition for *in situ* UHV scanning probe microscopy made very large molecules available for the study of their aggregation on surfaces [58–61]. For those molecules, the conformational freedom will be a key element for the self-assembly behavior [62–64].

References

[1] Gatteschi D, Sessoli R and Villain J 2006 *Molecular Nanomagnets* (Oxford: Oxford University Press)
[2] Bartolom J, Luis F and Fernndez J F 2013 *Molecular Magnets: Physics and Applications* (Berlin: Springer)
[3] Gatteschi D and Sessoli R 2003 *Angew. Chem. Int. Ed.* **42** 268
[4] Ishikawa N 2010 *Struct. Bond.* **135** 211
[5] Woodruff D N, Winpenny R E P and Layfield R A 2013 *Chem. Rev.* **113** 5110
[6] Ishikawa N, Sugita M, Ishikawa T, Koshihara S-y and Kaizu Y 2003 *J. Am. Chem. Soc.* **125** 8694
[7] Ishikawa N, Sugita M, Ishikawa T, Koshihara S and Kaizu Y 2004 *J. Phys. Chem.* B **108** 11265
[8] Ishikawa N, Sugita M and Wernsdorfer W 2005 *J. Am. Chem. Soc.* **127** 3650
[9] Ishikawa N, Sugita M and Wernsdorfer W 2005 *Angew. Chem.* **44** 2931

[10] Gonidec M, Davies E S, McMaster J, Amabilino D B and Veciana J 2010 *J. Am. Chem. Soc.* **132** 1756
[11] Gonidec M, Krivokapic I, Vidal-Gancedo J, Davies E S, McMaster J, Gorun S M and Veciana J 2013 *Inorg. Chem.* **52** 4464
[12] Bogani L and Wernsdorfer W 2008 *Nat. Mater.* **7** 179
[13] Urdampilleta M, Klyatskaya S, Cleuziou J-P, Ruben M and Wernsdorfer W 2012 *Nat. Mater.* **10** 502
[14] Vincent R, Klyatskaya S, Ruben M, Wernsdorfer W and Balestro F 2012 *Nature* **488** 357
[15] Thiele S, Balestro F, Ballou R, Klyatskaya S, Ruben M and Wernsdorfer W 2014 *Science* **344** 1135
[16] Gatteschi D *et al* 2009 *Inorg. Chem.* **48** 3408
[17] Cornia A *et al* 2011 *Chem. Soc. Rev.* **40** 3076
[18] Kahle S *et al* 2012 *Nano Lett.* **12** 518
[19] Stepanow S *et al* 2010 *J. Am. Chem. Soc.* **132** 11900
[20] Margheriti L *et al* 2010 *Adv. Mater* **22** 5488
[21] Gonidec M *et al* 2011 *J. Am. Chem. Soc.* **133** 6603
[22] Klar D, Candini A, Joly L, Klyatskaya S, Krumme B, Ohresser P, Kappler J, Ruben M and Wende H 2014 *Dalton Trans.* **43** 10686
[23] Mannini M *et al* 2014 *Nat. Commun.* **5** 4582
[24] Vitali L, Fabris S, Conte A M, Brink S, Ruben M, Baroni S and Kern K 2008 *Nano Lett.* **8** 3364
[25] Komeda T, Isshiki H, Liu J, Zhang Y-F, Lorente N, Katoh K, Breedlove B K and Yamashita M 2011 *Nat. Commun.* **2** 217
[26] Fu Y-S, Schwbel J, Hla S-W, Dilullo A, Hoffmann G, Klyatskaya S, Ruben M and Wiesendanger R 2012 *Nano Lett.* **12** 3931
[27] Robles R *et al* 2012 *Nano Lett.* **12** 3609
[28] Schwobel J *et al* 2012 *Nat. Commun.* **3** 953
[29] Fahrendorf S *et al* 2013 *Nat. Commun.* **4** 2425
[30] He Y, Zhang Y, Hong I-P, Cheng F, Zhou X, Shen Q, Li J, Wang Y, Jiang J and Wu K 2014 *Nano scale* **6** 10779
[31] Komeda T 2014 *ACS Nano* **8** 4866
[32] Mülegger S *et al* 2014 *Phys. Rev. Lett.* **113** 133001
[33] Löbbert G 2000 *Phthalocyanines Ullmannas Encyclopedia of Industrial Chemistry* 4th edn (Weinheim: Wiley-VCH)
[34] Horowitz G 1998 *Adv. Mater.* **10** 365
[35] Dimitrakopoulos C and Malenfant P 2002 *Adv. Mater.* **14** 99
[36] Bottari G, de la Torre G, Guldi D M and Torres T 2010 *Chem. Rev.* **110** 6768
[37] Hagfeldt A, Boschloo G, Sun L, Kloo L and Pettersson H 2010 *Chemical reviews* **110** 6595
[38] Kasuga K, Tsutsui M, Petterson R, Tatsumi K, van Opdenbosch N, Pepe G and Meyer E Jr 1980 *J. Am. Chem. Soc.* **102** 4835
[39] Moussavi M, De Cian A, Fischer J and Weiss R 1988 *Inorg. Chem.* **27** 1287
[40] Ishikawa N, Sugita M and Wernsdorfer W 2005 *Angew. Chem. Int. Ed.* **44** 2931
[41] Kyatskaya S, Mascarós J R G, Bogani L, Hennrich F, Kappes M, Wernsdorfer W and Ruben M 2009 *J. Am. Chem. Soc.* **131** 15143
[42] Cheng Z, Gao L, Deng Z, Jiang N, Liu Q, Shi D, Du S, Guo H and Gao H-J 2007 *J. Phys. Chem.* C **111** 9240
[43] Hipps K, Scudiero L, Barlow D E and Cooke M P 2002 *J. Am. Chem. Soc.* **124** 2126
[44] Karacuban H, Lange M, Schaffert J, Weingart O, Wagner T and Möller R 2009 *Surf. Sci.* **603** L39
[45] Wang Y, Ge X, Manzano C, Kröger J, Berndt R, Hofer W A, Tang H and Cerda J 2009 *J. Am. Chem. Soc.* **131** 10400
[46] Chang S-H, Kuck S, Brede J, Lichtenstein L, Hoffmann G and Wiesendanger R 2008 *Phys. Rev.* B **78** 233409
[47] Koike N, Uekusa H, Ohashi Y, Harnoode C, Kitamura F, Ohsaka T and Tokuda K 1996 *Inorg. Chem.* **35** 5798
[48] Lu X, Hipps K, Wang X and Mazur U 1996 *J. Am. Chem. Soc.* **118** 7197
[49] Lu X and Hipps K 1997 *J. Phys. Chem.* B **101** 5391
[50] Katoh K *et al* 2009 *J. Am. Chem. Soc.* **131** 9967
[51] Otsuki J, Komatsu Y, Kobayashi D, Asakawa M and Miyake K 2010 *J. Am. Chem. Soc.* **132** 6870
[52] van Daelen M, Li Y, Newsam J and van Santen R 1994 *Chem. Phys. Lett.* **226** 100
[53] Stepanow S, Lingenfelder M, Dmitriev A, Spillmann H, Delvigne E, Lin N, Deng X, Cai C, Barth J and Kern K 2004 *Nat. Mater.* **3** 229
[54] Stepanow S, Ohmann R, Leroy F, Lin N, Strunskus T, Woell C and Kern K 2010 *ACS Nano* **4** 1813
[55] Steiner T and Saenger W 1992 *J. Am. Chem. Soc.* **114** 10146
[56] Steiner T 2002 *Angew. Chem. Int. Ed.* **41** 48
[57] Tseng T-C *et al* 2010 *Nat. Chem.* **2** 374
[58] Rauschenbach S, Vogelgesang R, Malinowski N, Gerlach J W, Benyoucef M, Costantini G, Deng Z, Thontasen N and Kern K 2009 *ACS Nano* **3** 2901
[59] Hamann C, Woltmann R, Hong I-P, Hauptmann N, Karan S and Berndt R 2011 *Rev. Sci. Instr.* **82**
[60] Deng Z, Thontasen N, Malinowski N, Rinke G, Harnau L, Rauschenbach S and Kern K 2012 *Nano Lett* **12** 2452
[61] Rauschenbach S *et al* 2012 *Adv. Mater.* **24** 2761
[62] Thontasen N, Levita G, Malinowski N, Deng Z, Rauschenbach S and Kern K 2010 *J. Phys. Chem.* C **114** 17768
[63] Hauptmann N, Scheil K, Gopakumar T G, Otte F L, Schtt C, Herges R and Berndt R 2013 *J. Am. Chem. Soc.* **135** 8814
[64] Rinke G, Rauschenbach S, Harnau L, Albarghash A, Pauly M and Kern K 2014 *Nano lett.* **14** 5609